Japanese Journal of Applied Physics

REGULAR PAPER • **OPEN ACCESS**

Analysis of a second peak of electron density observed in high-power impulse magnetron sputtering plasma using a Langmuir probe

To cite this article: Kam-Hong Chau *et al* 2024 *Jpn. J. Appl. Phys.* **63** 016003

OPEN ACCESS

Japanese Journal of Applied Physics **63**, 016003 (2024) **REGULAR PAPER**

https://doi.org/**10.35848/1347-4065/ad13a5**

Analysis of a second peak of electron density observed in high-power impulse magnetron sputtering plasma using a Langmuir probe

Kam-Hong Chau[1,2*], Yoshinobu Kawai[3,4], Chi-Wai Kan[2], Jia-Lin Syu[1,3], Yen-Chun Liu[1,3], Ying-Hung Chen[1,3], Chen-Jui Liang[3,5], and Ju-Liang He[1,3]

[1]*Institute of Plasma, Feng Chia University, 100 Wenhwa Rd., Seatwen, Taichung 40724, Taiwan, Republic of China*
[2]*School of Fashion and Textiles, the Hong Kong Polytechnic University, Hung Hom, Kowloon, Hong Kong*
[3]*Department of Materials Science and Engineering, Feng Chia University, 100 Wenhwa Rd., Seatwen, Taichung 40724, Taiwan, Republic of China*
[4]*Interdisciplinary Graduate School of Engineering Sciences, Kyushu University, Kasugakoen 6-1, Kasuga, Fukuoka 816-8580, Japan*
[5]*International School of Technology and Management, Feng Chia University, 100 Wenhwa Rd., Seatwen, Taichung 40724, Taiwan, Republic of China*

*E-mail: edward.chau@connect.polyu.hk

Received July 15, 2023; revised October 29, 2023; accepted December 7, 2023; published online January 15, 2024

Plasma characteristics of a high-power impulse magnetron sputtering (HIPIMS) for copper deposition were investigated using a time-resolved Langmuir probe to explore HIPIMS discharge physics. Various discharge frequencies and pulse widths were employed while operating the HIPIMS in a constant current mode. Waveforms of the HIPIMS cathode current remained constant throughout the HIPIMS voltage pulse. It was found that electrons exhibited a bi-Maxwellian energy distribution both during and after the HIPIMS pulse. After the HIPIMS pulse, plasma density built up to a second peak while the bulk electron temperature quickly decreased. By examining the effect of pulse width and discharge frequency on the temperature of hot electrons through Langmuir *I–V* curves, it is suggested that the hot electron ionization contributed to the occurrence of the second peak. © 2024 The Author(s). Published on behalf of The Japan Society of Applied Physics by IOP Publishing Ltd

1. Introduction

High-power impulse magnetron sputtering (HIPIMS) plasma exhibits numerous interesting phenomena[1–13] characterized by its advantageous high electron density (n_e) and low electron temperature (T_e). However, the discharge physics of the HIPIMS plasma has not been fully understood. Multiple peaks observed in ion and electron densities of HIPIMS plasma are interesting observations. When a HIPIMS pulse width (T_{on}) is terminated, we would expect a decay of the charged particle densities. However, in addition to the initial density peak observed during the pulse, there were instances where subsequent peak(s) were observed after the pulse. These second peak or multiple peaks have previously been associated with ions[5,6] and electron currents/densities[1,3,4,7,8] after T_{on}. The pressure of argon working gas is a critical factor[3,5] influencing the presence of the second peak of plasma densities in the HIPIMS. Various theories have been proposed to explain the second peak or long tail phenomenon, including the involvement of the ion acoustic wave,[1,7] a backscattered wave,[5] and reflection of neutrals by the chamber wall.[9] However, a definitive conclusion regarding these second/multiple peaks phenomena has yet to be reached. In practice, comprehending the double or multiple plasma constitutes peaks in the HIPIMS plasma could contribute to optimizing the deposition rate, and even the production of a bi-polar HIPIMS plasma[14] by controlling the HIPIMS plasma parameters.

As is well known, metastable atoms are commonly found in the HIPIMS plasma. The abundance of the metastable atom can be similar to ions.[6,15] So the reserve of metastable atoms for ionization within the HIPIMS plasma is plentiful. Hopwood and Qian[16] reported that Penning ionization dominates at low electron densities, but electron-impact ionization becomes more significant at higher electron densities. Their model assumed a Maxwellian electron energy distribution function (EEDF). Penning ionization refers to an atom ionized by a metastable atom, in which the excitation energy of the metastable atom is larger than the ionization energy of the first atom.[17]

Anders[18] mentioned in his review paper that electrons have two different temperatures during the HIPIMS pulse because there are high-energy secondary electrons emitted from the target. However, the EEDF after the pulse is terminated was not described. Thus, it is an important subject to understand the EEDF in the HIPIMS plasma. Generally, the EEDF can be obtained from the Langmuir *I–V* curve. Usually, the Druyvesteyn method[4,7] is used to determine the EEDF, since this method may neglect the ion current contribution to the probe current. However, it is not easy to take the second derivative of the electron current against the probe voltage in the high-energy region with a digital method. Gudmundsson et al.[4] attempted to measure spatial and temporal characteristics of the HIPIMS plasma parameters using the Druyvesteyn method[4,7] and reported that the observed EEDF comprised two electron groups. The higher energy electrons have the so-called Druyvesteyn distribution where high-energy electrons are truncated. Pajdarova et al.[19] also reported that EEDF in the HIPIMS plasma followed a Druyvesteyn distribution.

A Langmuir probe is a versatile tool for plasma analysis.[20–22] In this study, we carefully examined time-resolved Langmuir *I–V* curves and EEDF of the HIPIMS plasma under varying T_{on} and discharge frequencies (f). It was found that high-energy electrons (hot electrons) co-exist with bulk electrons during the HIPIMS pulse voltage and after the HIPIMS pulse, that is, electrons have a bi-Maxwellian energy distribution function.[23]

2. Experimental methods

Figure 1 illustrates a schematic of the experimental apparatus.[24] In a grounded vacuum chamber, a rectangular

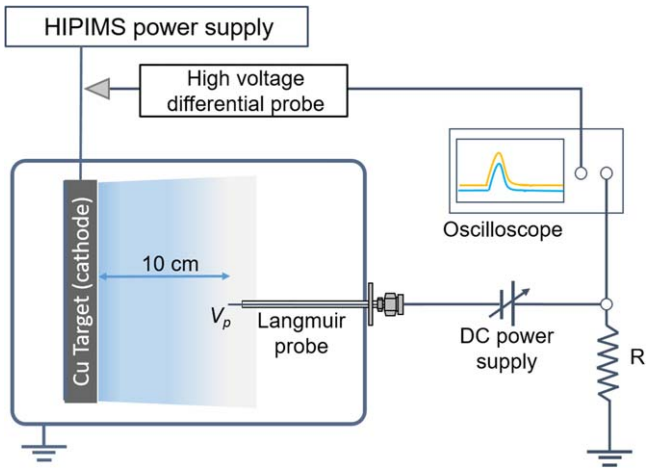

Fig. 1. Experimental apparatus. The Langmuir probe was subjected to various applied probe voltages (V_p) for conducting current measurement.[24)]

pure copper target with a 0.038 m^2 surface area was installed, and it had a racetrack area of 0.024 m^2. The target had permanent magnets attached to it. The north pole of the magnetic field is aligned with the center of the target, while the south pole to the edge of the target. A HIPIMS power supply (TRUMPF, Hüttinger TruPlasma Highpulse 4001) was connected to the copper target. The HIPIMS cathode voltage was monitored by a high-voltage differential probe (TECPEL, DP-25). A digital oscilloscope (GW Instek, GDS-2102E) then collected and recorded the cathode voltage signal from the differential probe. The HIPIMS power supply directly logged the HIPIMS cathode current. A total of five sets of power delivery parameters were employed in constant current mode at 150 A for HIPIMS. These parameters were purposely modified in relation to the values of f and T_{on}. The parameters were (1) $f = 400$ Hz, $T_{on} = 75$ μs, (2) $f = 400$ Hz, $T_{on} = 150$ μs, (3) $f = 400$ Hz, $T_{on} = 200$ μs, (4) $f = 600$ Hz, $T_{on} = 75$ μs and (5) $f = 800$ Hz, $T_{on} = 75$ μs. Argon was the working gas for the HIPIMS operations at a pressure of 0.16 Pa.

A home-made Langmuir probe was horizontally installed within the vacuum chamber to take time-resolved HIPIMS copper plasma measurements. The Langmuir probe was situated at a 100 mm distance from the copper target. The Langmuir probe was a tungsten wire with a diameter of 0.55 mm. The wire was shielded in an alumina tube, and the alumina tube was held by an earthed stainless steel tube. A 5 mm segment of the tungsten wire was not covered to establish contact with the copper plasma. On the other end, the wire was connected to the floating output of a DC power supply (IDRC, DSP-150-005HR) to enable adjustable DC biasing voltage. The tungsten wire, DC power supply, and a standard resistor were connected in series, forming a grounded circuit. A 20 Ω resistor was selected as the standard resistor for the cases where the DC power supply gave a negative voltage. Otherwise, under zero and positive voltage conditions, the standard resistor was changed to 10 Ω. The voltage across a standard resistor (V_R) was captured by the oscilloscope with 256-time averaging. Therefore, the Langmuir probe current (I), which is equal to the current though the resistor, is calculated from V_R and resistance value (R). The applied probe voltages (V_p) were slightly different from the DC power supply voltage V_b by the V_R, that is $V_p = V_b - V_R$. When the V_b was at positive bias 40 V, V_R had a magnitude of less than 5 V.

3. Results and discussion

As is well known, HIPIMS discharges were operated at a constant voltage mode by many researchers.[2,5,6,11–13)] We tried to produce a HIPIMS plasma at a constant voltage mode using our power supply. Figure 2 is a typical waveform of a HIPIMS discharge at a constant voltage of 800 V, where the pulse width is 75 μs and the discharge frequency is 400 Hz. The waveforms of the discharge voltage and current are similar to those in existing literature. However, we encountered a discrepancy in our experimental setup, while the cathode voltage output of the HIPIMS power supply was set at 800 V, the measured cathode voltage can only reach 550 V. Moreover, when the discharge voltage exceeded 800 V, the power supply shut off. This was because the sputtering target with a large racetrack for production, which led to an excessive discharge current. Therefore, we chose to employ the constant current mode for our investigation into the behaviors of a HIPIMS discharge plasma. Figure 3 illustrates a waveform of the resulting HIPIMS discharge in the constant current mode, with a T_{on} of 75 μs and f of 400 Hz. As seen in Fig. 3, the discharge current varies around 150 A during the HIPIMS voltage.

The study focused on analyzing the behavior of the HIPIMS discharge by studying HIPIMS parameters at different combinations of T_{on} and f using the Langmuir probe. Figure 4 is a typical Langmuir I–V curve at different time points, where T_{on} is 75 μs and f is 400 Hz. These curves were derived from I against time at various V_b. A knee clearly appears in the I–V curves, enabling easy determination of electron saturation current. Consequently, the electron density (n_e), bulk electron temperature (T_e), and hot electron temperature (T_e^h) were estimated over time by using the observed I–V curves. The analysis demonstrates that when the HIPIMS voltage pulse is applied, initially the electron current quickly increases, and reaches a maximum at around 50 μs, and decreases afterward. The ion saturation current can be found in the magnified section of Fig. 4. At 50 μs, the ion saturation current is −4.3 mA.

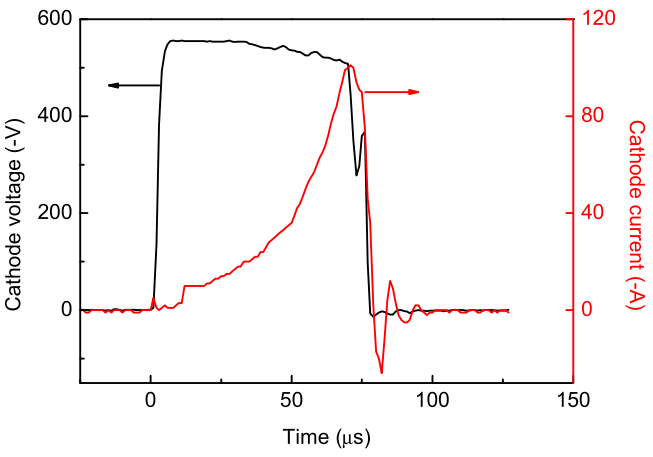

Fig. 2. Typical waveform of HIPIMS operations at a constant voltage mode, with a pulse width of 75 μs and a discharge frequency of 400 Hz.

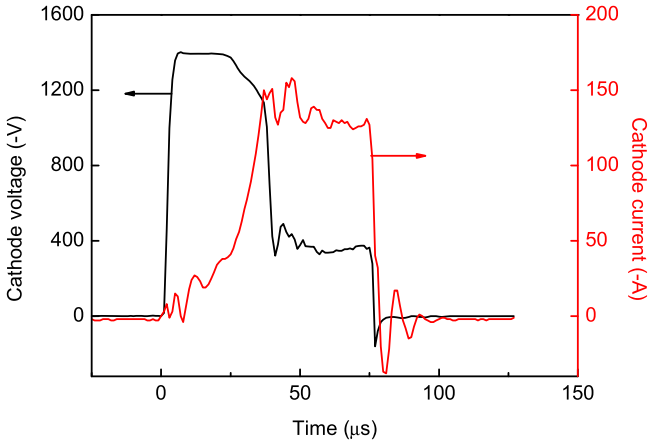

Fig. 3. Waveforms of HIPIMS operations at a constant current of 150 A, with a pulse width of 75 μs and a discharge frequency of 400 Hz.

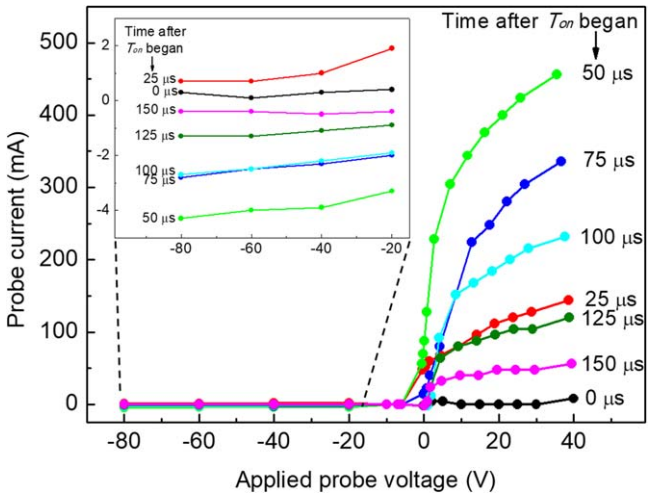

Fig. 4. Langmuir *I–V* curves in time, where the pulse width is 75 μs and frequency is 400 Hz. A negative applied probe voltage range of *I–V* curves is enlarged to show ion current.

The n_e can be determined from the *I–V* curves. Figure 5 shows typical temporal behaviors of the electron density for different pulse widths and frequencies.[24] As shown in Fig. 5, the second peak of the n_e appears. The second peak of density is comparable in magnitude to the first peak. Moreover, high electron density persists after the pulse has ended. The ion density was also estimated from the ion saturation current of the *I–V* curve, assuming that the dominant ions were Ar ions and Cu ions.[24] The second peak of the ion density appears at the time when the electron density peaked. Note that the second peak was observed at a low pressure of 0.16 Pa in our case, while the second peak was observed at a higher pressure in other studies.[1,6,8,22]

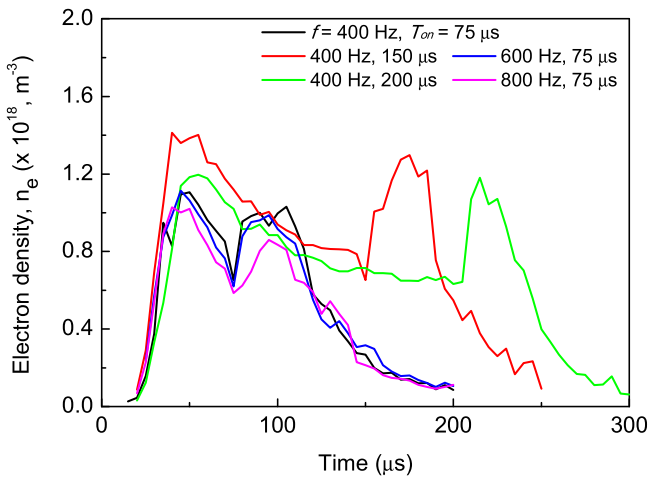

Fig. 5. Temporal behaviors of the electron density n_e under the different HIPIMS conditions.[24]

Some attempts[1,5,7,9] were made to explain the occurrence of a second peak of densities, and the second peak has been regarded as the chamber wall reflecting the neutrals.[9] If this explanation is correct, the second peak should be observed at low pressures because the mean free path is longer at low pressures. However, the second peak only appears at relatively higher pressure.[1,5]

In this experiment, we focused on examining an EEDF using the *I–V* curves, as we believe that the second peak is caused by electron collision ionization. Thus, we carefully examined the *I–V* curves to verify if the EEDF follows a Maxwellian distribution. Figure 6 shows typical semi-log plots of the *I–V* curves during T_{on} and after T_{on}, which clearly demonstrate that a bi-Maxwellian EEDF is observed in our experiments. The ion saturation current found in the *I–V* curves (Fig. 4) is removed from the semi-log plots, presenting a natural logarithm of electron current (I_e) on the *y*-axis.

It is commonly known that when the EEDF comprises two Maxwellians with distinct temperatures, as observed in our results, the two electron temperatures can be determined through linear fits on the semi-log *I–V* curve. Hoegy et al.[25] established the electron current of the probe, incorporating the electron drift velocity. We assume that the electron drift velocity is significantly smaller than the electron thermal velocity. When electrons exhibit isotropic distributions, specifically in the form of bi-Maxwellian with two electron temperatures, the electron current (I_e) is calculated as

$$I_e = (1/4)n_e eAv_{th}\exp(-eV/kT_e) + (1/4)n_e^h eAv_{th}^h \exp(-eV/kT_e^h). \quad (1)$$

Here, n_e and n_e^h represent the density of bulk and hot electrons respectively, while v_{th} and v_{th}^h denote the thermal velocity of bulk and hot electrons. V represents the difference between the plasma potential and the probe voltage and A is the area of the probe. The derivation of the bulk electron term of Eq. (1) can find[24] for detail, the derivation of the hot electron term is similar to the bulk one.

In general, obtaining the EEDF provides more comprehensive results. However, as we have explained earlier, it is challenging to obtain EEDF over a wide energy range using the commercially available second derivative method. In fact, many researchers measured the EEDF of HIPIMS plasma, which consistently exhibits a Druyvesteyn distribution. This result arises from the use of the commercial second derivative method, which is only applicable within a narrow energy range. Therefore, we believe that our custom-made probe is more advantageous for measuring the parameters of HIPIMS plasma.

T_e is calculated from the slope of the semi-log *I–V* plot, where the slope is clear to be identified since T_{on} at 20 μs. From approximately 50 μs, the tail of the hot electron becomes evident on the semi-log *I–V* plot. This tail sustains for around 20 to 30 μs after the HIPIMS pulse is off. The T_e values are calculated from the slope of semi-log *I–V* plots [Figs. 6(a)–6(c)] during T_{on} is around 2 eV. At the same time,

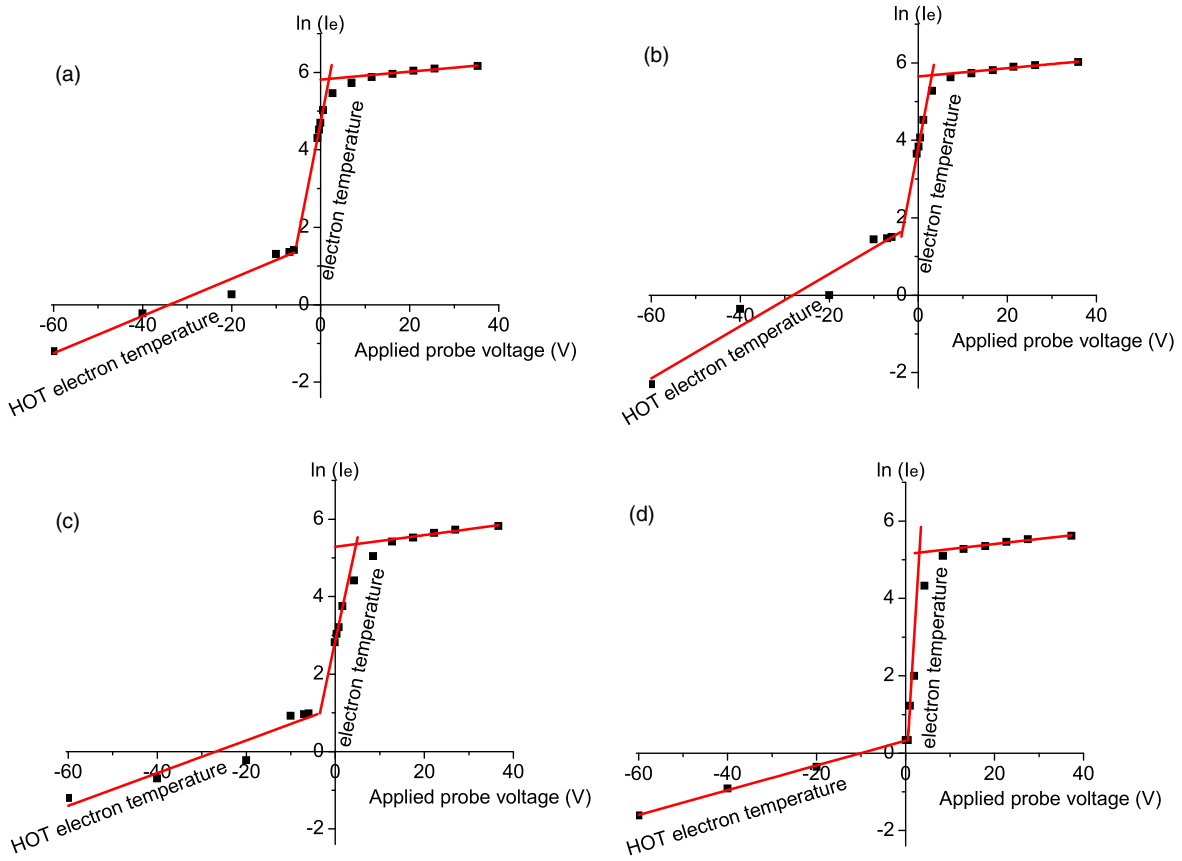

Fig. 6. Typical semi-log *I–V* curves (a) at 45 μs, (b) at 60 μs, (c) at 75 μs, and (d) at 90 μs. The HIPIMS operated with T_{on} 75 μs and f 400 Hz.

high-energy electrons (hot electrons) co-exist, indicating bi-Maxwellian electron energy distribution during the HIPIMS pulse. Figure 6(d) shows that T_e after T_{on} is very low (<1 eV) and hot electrons co-exist, therefore, electron energy distributes bi-Maxwellian after the HIPIMS pulse. As mentioned by Anders,[12] the secondary electrons emitted from the target due to ion bombardment have energy in the range of hundreds of electronvolt. These secondary electrons contribute to ionization and excitation in the HIPIMS discharge. Since these secondary electrons lose their energy in the plasma, they can be collected by the Langmuir probe.

In this study, we estimated temporal behaviors of the electron temperature from the semi-log Langmuir *I–V* curves. The results are shown in Fig. 7, assuming Maxwellian distribution for both T_e and T_e^h. During the HIPIMS pulse, T_e is found to be approximately 2 eV. When the pulse is off, T_e rapidly decreases to below 1 eV in microseconds. Figure 7 shows that both the frequency and the pulse width are important parameters. When the frequency is increased, the T_e^h during the HIPIMS pulse decreases; T_e^h is around 20 eV at f equal to 400 Hz and decreases to around 6 eV at other frequencies. In addition, T_e^h depends on the pulse width as well. These findings suggest that both the frequency and pulse width play an important role in controlling the discharge behavior of the HIPIMS. The detailed mechanism is to be explained by conducting experiments and work in the future. Carefully looking at Fig. 7, T_e^h can raise to around 10 eV, when the pulse width exceeds 100 μs. T_e^h becomes not measurable after the pulse ended for about 20 μs, which

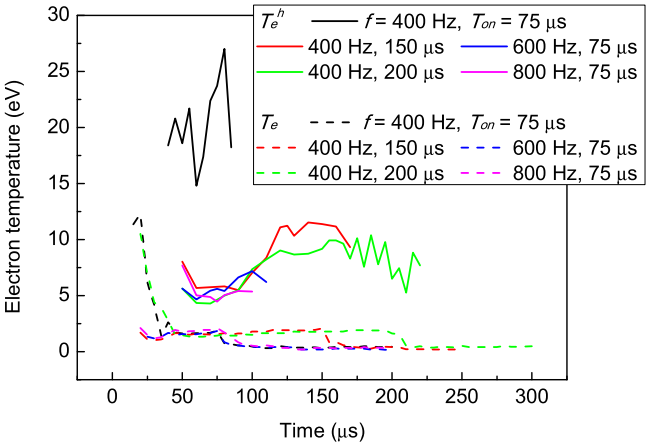

Fig. 7. Temporal behaviors of the electron temperature for different pulse widths and frequencies. Solid lines and dash lines represent hot electrons and bulk electrons, respectively.

coincides with the time of the second peak of bulk electron density shown in Fig. 5. Consistently in this study, we have observed the presence of the second peak. It is widely recognized that the HIPIMS discharge produces a plasma that is fully ionized. In general, high-energy electrons play a significant role in the process of ionization. Further discussion regarding the ionization phenomenon is presented in the following paragraphs.

Figure 5 shows that when the HIPIMS pulse is off, the electron density rapidly decreases before the second peak appears. This suggests Penning ionization should occur[26] at

low n_e. Penning ionization was discussed in plasmas with electrons exhibiting a Maxwellian energy distribution.[16] In our case, electrons have a bi-Maxwellian energy distribution. Thus, we conclude that Penning ionization may contribute to the formation of the second peak. Recently, simulations about low-temperature plasma are in progress, so the simulation for the HIPIMS discharge may be helpful for clarifying the effect of Penning ionization on the second peak.

The ionization rate constant $K = \langle \sigma_i v_e \rangle$[16,27] is an important parameter in plasma production, where σ_i is the ionization cross section and v_e is the electron thermal velocity. When EEDF is Maxwellian, K is expressed in terms of the kinetic energy ε as,

$$\langle \sigma v_e \rangle_i = \sqrt{8/\pi m_e}\,(kT)^{-3/2} \int_0^\infty \sigma_i(\varepsilon)\varepsilon \exp(-\varepsilon/kT)d\varepsilon \qquad (2)$$

In the above equation, k is the Boltzmann constant and m_e is the electron mass. The rate constant K indicates that hot electrons with energy higher than the ionization energy are responsible for ionization. Lieberman and Lichtenberg[28] calculated K for argon plasma. According to their result, when T_e increases from 2 eV to 10 eV, the rate constant at 10 eV is three-orders of magnitude higher than that at 2 eV.[28] Thus, we can conclude that EEDF has a bi-Maxwellian distribution that generates the second peak of densities. Therefore, the second peak is a result of ionization caused by the hot electrons. The HIPIMS plasma is produced at low pressure, so electron collisions with neutral argon atoms are negligible. As already reported by Anders,[12] electron Coulomb collisions dominate in the HIPIMS plasma. Electrons accelerated by the cathode sheath contribute to the HIPIMS discharge and lose their energy. However, some high-energy electrons can exist due to fewer collisions and their extended lifetime.[29] High-energy electrons can be analyzed by using an energy analyzer can be a future investigation.

As already described in Sect. 1, the temporal behavior of the HIPIMS plasma has been investigated by numerous researchers using the Druyvesteyn method. Obtained EEDF consisted of two groups of energy, and high-energy electrons had a Druyvesteyn EEDF. On the other hand, we observed a bi-Maxwellian EEDF during and after the HIPIMS pulse. This difference is considered to be due to analyzing the energetic region. We measured a probe current and voltage with a digital oscilloscope that has better energy resolution. Reported EEDFs were plotted against up to 10 V. However, Fig. 6 shows that our measurements have a broad energy region.

A bi-polar HIPIMS,[14,30–34] applying a reverse positive pulse at the end of the negative pulse during the HIPIMS discharge, is gaining a great deal of interest. However, there are few reports regarding the relationship between the reverse positive voltage pulse parameter and the behavior of HIPIMS plasma. As described, hot electrons have extended lifetime, suggesting their potential role in producing the second peak, which acts as a pre-ionized plasma during the positive voltage phase. Therefore, the second peak may contribute to the bi-polar HIPIMS plasma production.

4. Conclusions

The HIPIMS plasma was examined through temporal measurements using the time-resolved Langmuir probe, leading to several findings:

(1) Electrons have a bi-Maxwellian energy distribution function after the HIPIMS pulse on time as well as during the pulse.
(2) Hot electron temperature depends on the discharge frequency and the pulse width, suggesting HIPIMS plasma parameters can be controlled through the discharge frequency and pulse width.
(3) Hot electrons contributed to the production of the second peak of plasma density after the pulse is terminated.

In conclusion, the results reveal that electrons of the HIPIMS plasma have a bi-Maxwellian energy distribution, and the high-energy electrons (hot electrons) are responsible for the occurrence of the second peak. To clarify the detailed role of the hot electrons in the HIPIMS discharge, a direct measurement of the hot electrons may be important and will be considered as a future subject.

ORCID iDs

Kam-Hong Chau https://orcid.org/0000-0002-3192-3938

1) J. Alami, J. T. Gudmundsson, J. Bohlmark, J. Birch, and U. Helmersson, Plasma Sources Sci. Technol. **14**, 525 (2005).
2) B. Liebig, N. S. J. Braithwaite, P. J. Kelly, R. Chistyakov, B. Abraham, and J. W. Bradley, Surf. Coat. Technol. **205**, S312 (2011).
3) A. Vetushka and A. P. Ehiasarian, J. Phys. D: Appl. Phys. **41**, 015204 (2008).
4) J. T. Gudmundsson, J. Alami, and U. Helmersson, Appl. Phys. Lett. **78**, 3427 (2001).
5) D. Horwat and A. Anders, J. Appl. Phys. **108**, 123306 (2010).
6) J. Hnilica, P. Klein, P. Vašina, R. Snyders, and N. Britun, J. Appl. Phys. **128**, 043303 (2020).
7) J. T. Gudmundsson, J. Alami, and U. Helmersson, Surf. Coat. Technol. **161**, 249 (2002).
8) A. P. Ehiasarian, A. Vetushka, A. Hecimovic, and S. Konstantinidis, J. Appl. Phys. **104**, 083305 (2008).
9) J. T. Gudmundsson, N. Brenning, D. Lundin, and U. Helmersson, J. Vac. Sci. Technol. A **30**, 030801 (2012).
10) J. T. Gudmundsson, P. Sigurjonsson, P. Larsson, D. Lundin, and U. Helmersson, J. Appl. Phys. **105**, 123302 (2009).
11) A. Anders, J. Čapek, M. Hála, and L. Martinu, J. Phys. D: Appl. Phys. **45**, 012003 (2012).
12) A. Anders, P. Ni, and A. Rauch, J. Appl. Phys. **111**, 053304 (2012).
13) A. Hecimovic and A. P. Ehiasarian, J. Phys. D: Appl. Phys. **42**, 135209 (2009).
14) R. P. B. Viloan, J. Gu, R. Boyd, J. Keraudy, L. Li, and U. Helmersson, Thin Solid Films **688**, 137350 (2019).
15) N. Britun, S. Konstantinidis, and R. Snyders, Plasma Processes Polym. **12**, 1010 (2015).
16) J. Hopwood and F. Qian, J. Appl. Phys. **78**, 758 (1995).
17) D. M. Mattox, *Handbook of Physical Vapor Deposition (PVD) Processing* (William Andrew Publishing, Boston, MA, 2010) 2nd ed. p. 162.
18) A. Anders, J. Appl. Phys. **121**, 171101 (2017).
19) A. D. Pajdarová, J. Vlček, P. Kudláček, and J. Lukáš, Plasma Sources Sci. Technol. **18**, 025008 (2009).
20) R. L. Merlino, Am. J. Phys. **75**, 1078 (2007).
21) M. Moriyama, N. Nakahara, A. Mitsuya, H. Suzuki, K. Kurihara, D. Iino, H. Fukumizu, and H. Toyoda, Jpn. J. Appl. Phys. **59**, SJJB03 (2020).
22) P. J. Ryan, J. W. Bradley, and M. D. Bowden, Phys. Plasmas **26**, 040702 (2019).
23) V. A. Godyak and V. I. Demidov, J. Phys. D: Appl. Phys. **44**, 233001 (2011).

24) K.-H. Chau, Y. Kawai, C.-W. Kan, J.-L. Syu, Y.-C. Liu, Y.-H. Chen, C.-J. Liang, and J.-L. He, Jpn. J. Appl. Phys. **61**, SA1020 (2022).
25) W. R. Hoegy and L. H. Brace, Rev. Sci. Instrum. **70**, 3015 (1999).
26) M. Palmucci, N. Britun, T. Silva, R. Snyders, and S. Konstantinidis, J. Phys. D: Appl. Phys. **46**, 215201 (2013).
27) M. A. Lieberman and A. J. Lichtenberg, *Principles of Plasma Discharges and Materials Processing* (Wiley, Hoboken, NJ, 2005) 2nd ed. p. 72.
28) M. A. Lieberman and A. J. Lichtenberg, *Principles of Plasma Discharges and Materials Processing* (Wiley, Hoboken, NJ, 2005) 2nd ed. p. 80.
29) J. Hnilica, P. Klein, P. Vašina, R. Snyders, and N. Britun, J. Appl. Phys. **128**, 043304 (2020).
30) B. Wu, I. Haehnlein, I. Shchelkanov, J. McLain, D. Patel, J. Uhlig, B. Jurczyk, Y. Leng, and D. N. Ruzic, Vacuum **150**, 216 (2018).
31) N. Britun, M. Michiels, T. Godfroid, and R. Snyders, Appl. Phys. Lett. **112**, 234103 (2018).
32) I.-L. Velicu, G.-T. Ianoş, C. Porosnicu, I. Mihăilă, I. Burducea, A. Velea, D. Cristea, D. Munteanu, and V. Tiron, Surf. Coat. Technol. **359**, 97 (2019).
33) J. Keraudy, R. P. B. Viloan, M. A. Raadu, N. Brenning, D. Lundin, and U. Helmersson, Surf. Coat. Technol. **359**, 433 (2019).
34) M. Michiels, T. Godfroid, R. Snyders, and N. Britun, J. Phys. D: Appl. Phys. **53**, 435205 (2020).